J Solid State Electrochem (2012) 16:3349–3354
DOI 10.1007/s10008-012-1780-x

ORIGINAL PAPER

Preparation and characterization of NASICON type Li^+ ionic conductors

Rayavarapu Prasada Rao · Chen Maohua · Stefan Adams

Received: 26 August 2011 / Revised: 15 May 2012 / Accepted: 17 May 2012 / Published online: 26 May 2012

Abstract The new scandium/aluminium co-doped NASICON phases $Li_{1+x}Al_ySc_{x-y}Ti_{2-x}(PO_4)_3$ (x=0.3, y= 0,0.1,0.2,0.3) were prepared by mechanical milling followed by annealing of the mixtures at 950 °C. X-ray diffraction of all samples showed the formation of NASICON structure with space group R-3c along with a minor impurity. Rietveld refinement of the X-ray data was performed to identify the structural variation. Doping with Sc^{3+} caused elongation of *a*- and *c*- axes for all the compounds when compared with undoped $LiTi_2(PO_4)_3$. The compound $Li_{1.3}Sc_{0.3}Ti_{1.7}(PO_4)_3$ showed a maximum of a=8.5504(7), c=20.986(3) Å at room temperature and exhibited highest coefficient of thermal expansion. The highest ionic conductivity (σ), 7.28×10^{-4} S cm^{-1} was observed for $Li_{1.3}Sc_{0.3}Ti_{1.7}(PO_4)_3$, two orders of magnitude higher than for the undoped phase.

Keywords NASICON · Lithium ion conduction · Bond valence · Ion transport · Temperature dependent X-ray

Introduction

Rechargeable all-solid-state lithium (Li)- or Li-ion batteries are attractive power sources for applications, like 'smart' credit cards and medical implants. They need a Li-fast ion conductor as the solid electrolyte. Compared to the significant and successful efforts on glassy lithium ionic conductors that led to materials suitable for all-solid-state lithium battery, little effort has been devoted into material developments concerning crystalline lithium ionic conductors during the last decade. On the other hand, crystalline ionic conductors have a number of advantages in conductivity and stability over glassy or polymer systems, i.e. crystalline copper and silver ionic conductors show extremely high conductivities even at room temperature, but no comparable "superionic" lithium solid electrolytes have been identified so far. Materials design of crystalline ionic conductors are based on certain structural criteria: (a) mobile ions should have a suitable size for conduction pathways in the lattice, (b) there should be disorder in the mobile ion sublattice, and (c) highly polarizable mobile ion and counterion sublattices are preferable. "Lithium superionic conductor" LISICON $[Li_{14}Zn(GeO_4)_4]$ is an example of a material which was designed using the above criteria. Many compounds with the same type of framework have been reported in the literature (see, e.g. [1–3]) and a wide range of solid solutions formed by aliovalent substitutions (introducing interstitial lithium ions or vacancies) led to high ionic conductivities at elevated temperatures. The conductivity values at room temperature ($\approx10^{-6}$ S/cm for $Li_{3.6}Si_{0.6}P_{0.4}O_4$, for example) are however still by far lower than those of copper and silver ionic conductors.

In order to further enhance the ionic conductivity of these materials, glass ceramics have been explored which for Li_2O-Al_2O_3-GeO_2-P_2O_5 result in Li^+ ion conductivities of about 10^{-4} S/cm at room temperature [4, 5]. The high ionic conductivity of such glass ceramics was ascribed to the interface region between glassy and crystalline phases [6].

The high cation mobility and thermal stability of NASICON double phosphates allow us to consider them as

Contribution to ICMAT 2011, Symposium N: "Advanced Materials for Energy Storage Systems—From Fundamentals to Applications", June 26th–July 1st 2011, Singapore

R. P. Rao (✉) · C. Maohua · S. Adams
Department of Materials Science and Engineering, National University of Singapore,
Singapore 117576, Singapore
e-mail: mserpr@gmail.com

potential materials for use in electrochemical devices. $LiTi_2(PO_4)_3$ with NASICON structure is built of two TiO_6 octahedra linked via shared oxygen atoms with three PO_4 tetrahedra. Doping by M = Al, Sc, Y, Fe, or Cr has been shown to be effective in enhancing Li^+ ion transport in the NASICON-type phases $Li_{1+x}M_xTi_{2-x}(PO_4)_3$. The influence of substituting Ti^{4+} to Sc^{3+} or Al^{3+} on structure and electric properties of the host compound $LiTi_2(PO_4)_3$ provided was discussed in [7]. The lattice parameters and conductivity of rhombohedral $Li_{1+x}Sc_x$(or)$Al_xTi_{2-x}(PO_4)_3$ (where x=0–0.3) depend on stoichiometric factor x; the maximum overall ionic conductivity at room temperature was found to be $\sigma=7\times10^{-4}$ S cm^{-1} for Al and x=0.3 [7].

In this work we aim at the preparation of $Li_{1+x}Al_ySc_{x-y}Ti_{2-x}(PO_4)_3$ (x=0.3, y=0, 0.1, 0.2, 0.3) crystalline compounds and understanding the link between the variations in structure variation of lattice parameters and ionic conductivity combining the experimental study with simple bond valence models of changes in the lithium ion transport pathways induced by the studied dopants.

Sample preparation and properties characterization

$Li_{1.3}Al_{0.3}Ti_{1.7}(PO_4)_3$ (LA3T), $Li_{1.3}Al_{0.2}Sc_{0.1}Ti_{1.7}(PO_4)_3$ (LA2ST), $Li_{1.3}Al_{0.1}Sc_{0.2}Ti_{1.7}(PO_4)_3$ (LAS2T) and $Li_{1.3}Sc_{0.3}Ti_{1.7}(PO_4)_3$ (LS3T) polycrystalline electrolytes were prepared using analytical grade Li_2CO_3, $NH_4H_2PO_4$, TiO_2, Sc_2O_3, $Al(OH)_3$ as starting materials. The starting materials were mechanically milled using an 85-ml zirconium bowl with 25 balls of 10 mm ø for 5 h at a speed of 300 rpm. The mixtures were heated in a platinum crucible at 950 °C for 18 h to remove all the volatile products and cooled to room temperature with natural cooling rate. The obtained samples were ground manually into fine powder. The samples were then characterized using X-ray powder diffractometry operated with Cu K_α radiation (PANalytical X'Pert PRO) equipped with a fast linear detector (X'Celerator). XRD data were collected in the 2θ range 10–100° with a nominal scan rate of 160 s/step and a step size of 0.017° in the temperature range of 30 °C to 350 °C. Rietveld refinements of XRD powder patterns are performed with the Generalized Structure Analysis System by Larson and von Dreele [8] along with the graphical user interface EXPGUI. Structure data from published neutron diffraction measurements by Alami et al. [9] for $LiTi_2(PO_4)_3$ was used as the starting point of the refinement. Ionic conductivity measurements of the final samples different temperatures were carried out by impedance spectroscopy (Schlumberger Solartron SI1260) in the frequency range of 1 Hz to 1 MHz using sputtered gold (500 Å thick) as electrodes. At each temperature, the samples were kept for 20 min for thermal equilibration. The bulk resistance R_b was determined from fitting an equivalent circuit consisting of C_b, R_b and a Warburg element to the impedance data. SEM photographs are collected for the same sample pellets used for the ionic conductivity study to clarify their morphology (JEOL JSM-6700F). In order to understand the transport mechanism of mobile ions in these systems bond valence (BV) calculations were applied to $LiTi_2(PO_4)_3$. A brief outlook of the BV approach is given below; for more details, the reader is referred to our previous publications [10–17].

Bond valence approach

Empirical relationships between bond length, R, and bond valence, s, given by

$$s_{Li-O} = \exp\left[\left(\frac{R_0 - R}{b}\right)\right] \quad (1)$$

are widely used in crystal chemistry to identify equilibrium atomic sites as regions within a structure, where the bond valence (BV) sum of the atom approximately equals its oxidation state. In the case of Lithium solid electrolytes, the empirical BV parameters (R_0=1.17 Å, b=0.516 Å [11]) permit to identify low energy interstitial sites as sites, where the interactions with all neighbouring oxygen anions yields approximately the BV sum 1. While bond valences, $s_{Li\text{-}O}$, and hence the BV sum mismatch $|\Delta V|$ are mostly expressed in arbitrary "valence units", they may—as we have shown recently—[14–17] be linked to an absolute energy scale by expressing the bond valence as a Morse-type interaction energy, E, given by:

$$E = D_0\left\{\frac{(s - s_{\min})^2}{s_{\min}^2} - 1\right\} = D_0\left(s_{rel}^2 - 2s_{rel}\right) \quad (2)$$

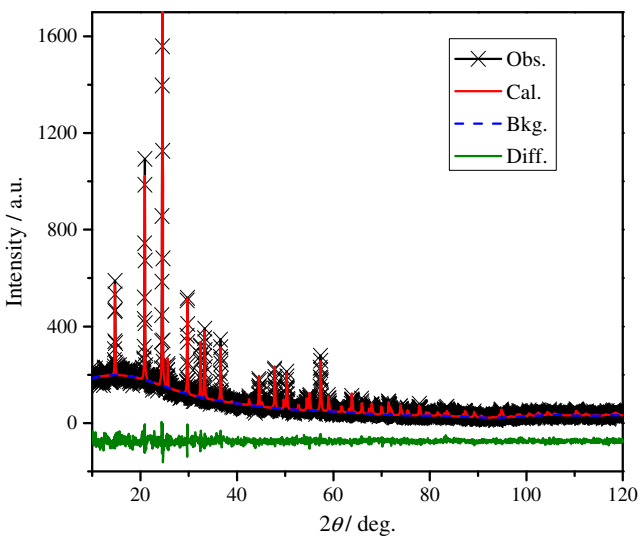

Fig. 1 Rietveld refinement of $Li_{1.3}Al_{0.3}Ti_{1.7}(PO_4)_3$

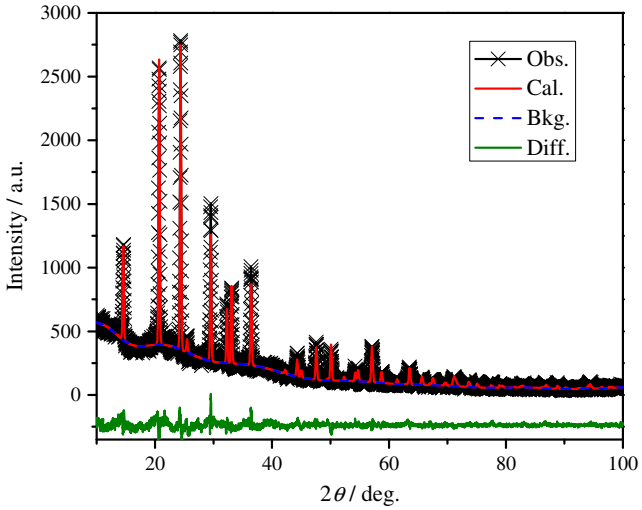

Fig. 2 Rietveld refinement of $Li_{1.3}Al_{0.2}Sc_{0.1}Al_{0.2}Ti_{1.7}(PO_4)_3$

here, $s_{rel} = s/s_{min}$, where s_{min} represents the BV for the equilibrium distance, R_{min}. R_{min} as well as the bond breaking energy D_0 are estimated from the tabulated BV parameters and the typical coordination number of the cation, N_C [15]. Note that the equilibrium distance R_{min} is thus in general different from R_0, the distance corresponding to a bond valence value of $s=1$.

The modelling of pathways for mobile Li^+ as regions of low site energy E(Li) (or of low BV sum mismatch, $|\Delta V(\text{Li})|$) connecting equilibrium and interstitial sites has been shown to provide a simple and reliable way of identifying transport pathways in local structure models, provided that the local structure model captures the essential structural features [17]. As described more in detail in our previous reports [13, 15], pathways for Li^+ can be visualized as regions enclosed by isosurfaces of constant E(Li) based on a grid of E(Li) values with a resolution<0.1 Å covering the unit cell. The threshold value of E(Li), for which the E(Li) isosurfaces form a continuous migration pathway (that includes both occupied and vacant Li sites), allows for a rough estimate of the activation energy for the Li^+ ion transport process.

Results and discussions

X-ray diffraction patterns of $Li_{1.3}Al_{0.3}Ti_{1.7}(PO_4)_3$, $Li_{1.3}Al_{0.2}$ $Sc_{0.1}Ti_{1.7}(PO_4)_3$, $Li_{1.3}Al_{0.1}$ $Sc_{0.2}Ti_{1.7}(PO_4)_3$, $Li_{1.3}Sc_{0.3}Ti_{1.7}(PO_4)_3$ showed crystalline nature of samples with *R-3c* space group, commonly known as NASICON phase. In the subsequent description we generally refer to the hexagonal setting of this space group. Diffraction patterns for the $Li_{1.3}Al_{0.2}Sc_{0.1}Ti_{1.7}(PO_4)_3$ sample showed a low intensity peak indicating the possibility of a minor secondary phase matching with TiP_2O_7. Matching of the peak positions for all these compounds with the reported NASICON structure for $LiTi_2(PO_4)_3$ indicates the successful doping of Sc_3^+ and Al_3^+. As example, Figs. 1 and 2 show the Rietveld refinements of $Li_{1.3}Al_{0.3}Ti_{1.7}(PO_4)_3$ and $Li_{1.3}Al_{0.2}Sc_{0.1}$-$Ti_{1.7}(PO_4)_3$. The parameters resulting from the Rietveld refinements for the compounds under study are summarized and compared with undoped $LiTi_2(PO_4)_3$ in Table 1. A 15 % replacement of Ti^{4+} (ionic radius 0.605 Å) by Al^{3+} (ionic radius 0.535 Å) reduced the volume of unit cell, when compared with $LiTi_2(PO_4)_3$, whereas doping with Sc^{3+} (ionic radius 0.745 Å) increased the volume of the cell. Figure 3 shows the variation of lattice parameters and volume with temperature. Lattice parameter *c*-axis and volume *V* show increase monotonically till 350 °C (see Fig. 3b and c), but the *a*-axis showed non-linear expansion. The coefficient of thermal expansion is more for $Li_{1.3}Sc_{0.3}Ti_{1.3}(PO_4)_3$. Figure 4 shows as a representative example the dense morphology of the $Li_{1.3}Sc_{0.1}Al_{0.2}Ti_{1.7}(PO_4)_3$ sample consisting of an irregular orientation of isometric crystals of sizes ranging from 0.2–3 μm.

Nyquist plots are obtained from impedance spectroscopy at selected temperatures and are fitted with equivalent circuit to determine the bulk resistance. The Arrhenius-type temperature dependence of the conductivity (σ) for all the compounds under investigation, as derived from these impedance measurements, is summarized in the graph of Fig. 5. The activation energy (E_a) of $Li_{1.3}Sc_{0.3}Ti_{1.7}(PO_4)_3$ is 0.26 eV and is lowest among the compounds prepared

Table 1 Lattice constants for all the compounds from Rietveld refinement of X-ray powder diffraction data

Compound	*a* (Å)	*c* (Å)	*V* (Å^3)	α_L (K^{-1}) (*a*-axis)	α_L (K^{-1}) (*c*-axis)	α_V (K^{-1})
$LiTi_2(PO_4)_3$[a]	8.5045(5)	20.9510(3)	1,312.3	–	–	–
$Li_{1.3}Al_{0.3}Ti_{1.7}(PO_4)_3$	8.500(1)	20.820(5)	1,302.8(7)	4.30×10^{-7}	3.18×10^{-5}	2.78×10^{-5}
$Li_{1.31}Al_{0.2}Sc_{0.1}$ $Ti_{1.7}(PO_4)_3$	8.5216(6)	20.917(2)	1,315.4(2)	5.91×10^{-6}	2.39×10^{-5}	3.81×10^{-5}
$Li_{1.3}$ $Al_{0.1}Sc_{0.2}Ti_{1.7}(PO_4)_3$	8.5244(6)	20.925(2)	1,316.8(2)	2.22×10^{-6}	3.02×10^{-5}	3.47×10^{-5}
$Li_{1.3}Sc_{0.3}Ti_{1.7}(PO_4)_3$	8.5504(7)	20.986(3)	1,328.7(2)	5.31×10^{-6}	3.60×10^{-5}	4.68×10^{-5}

[a] Data from literature [10]

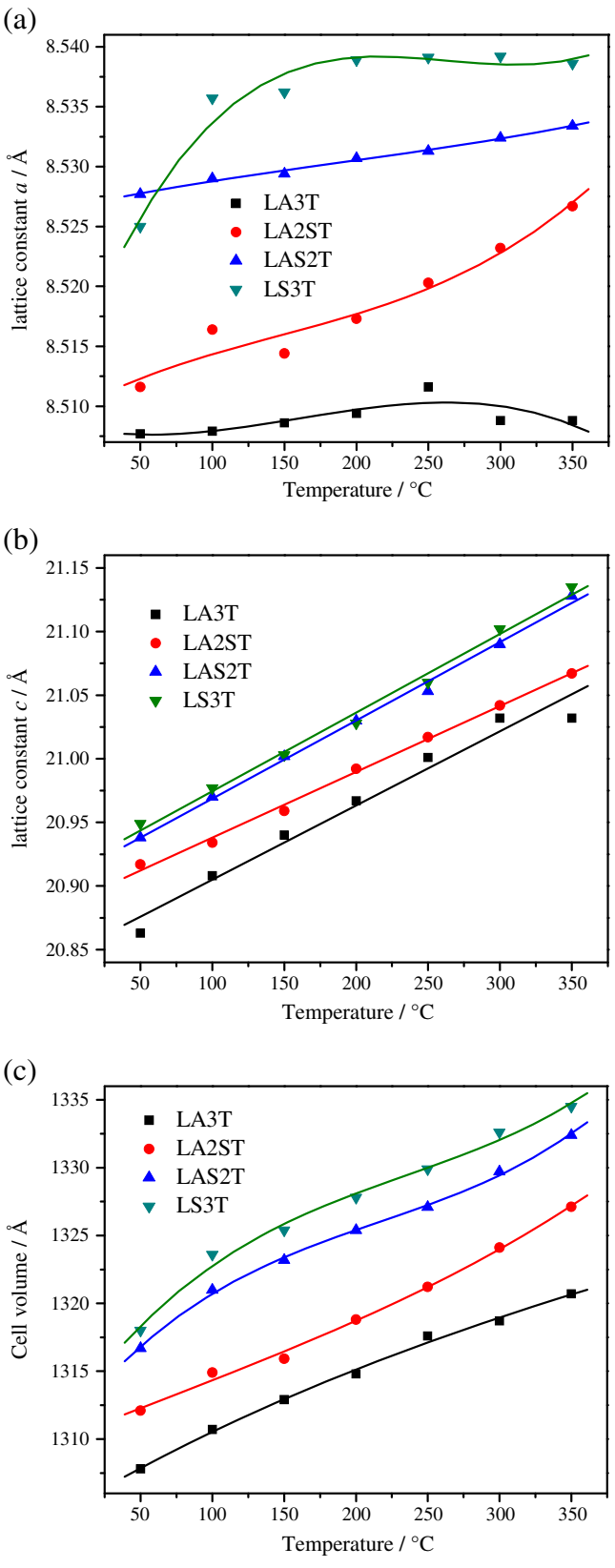

Fig. 3 Variation of lattice parameters **a** *a*-axis, **b** *c*-axis, and **c** volume with temperature

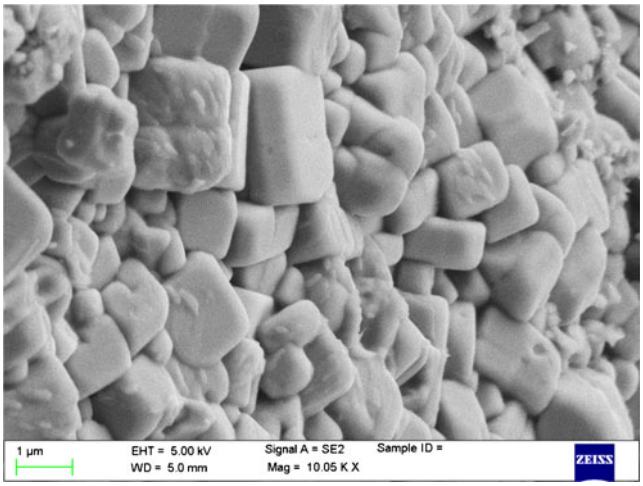

Fig. 4 SEM image of $Li_{1.3}Sc_{0.1}Al_{0.2}Ti_{1.7}(PO_4)_3$

with room temperature ionic conductivity 7.28×10^{-4} (see Table 2). The inset in Fig. 5 highlights that the variation of room temperature conductivity with the co-doping of Sc^{3+} is non-linear: compositions containing both dopants exhibit a lower conductivity than what could be expected from the interpolation of the two limiting single dopant cases. The detailed origin of such a mixed dopant effect will require further studies.

Figure 6 visualizes the structure of $Li_1Ti_2(PO_4)_3$, interstitial Li sites and the Li^+ ion transport pathways as calculated using our BV approach. The $LiTi_2(PO_4)_3$ structure is built of two TiO_6 octahedra linked via shared oxygen atoms with three PO_4 tetrahedra. In the ordered undoped structure, the Li ions fully occupy the regular I1 sites on the inversion centre octahedrally coordinated by 6 O atoms. The Li transport pathways connect two I1 sites via an interstitial site I2

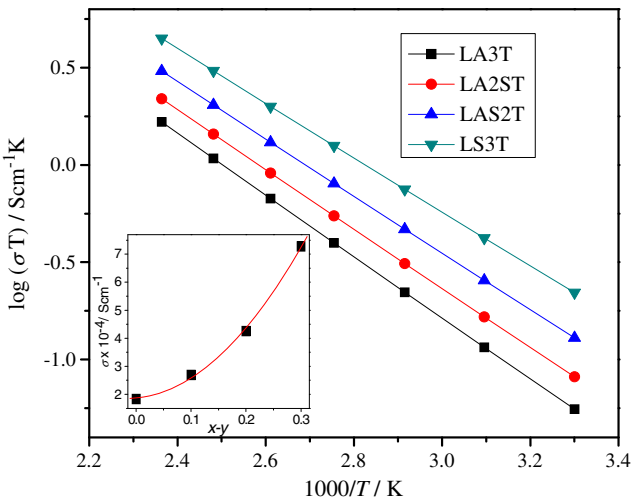

Fig. 5 Variation of ionic conductivity with temperature of NASICON compounds and variation of ionic conductivity at room temperature with the increase of Sc content (*x*–*y*) (*inset*)

Table 2 Physical parameters of compounds under investigation

Compound	σ at 25 °C (S/cm)	E_a (Exp.) (eV)	E_a (BV) (eV)
$Li_{1.3}Al_{0.3}Ti_{1.7}(PO_4)_3$	1.83×10^{-4}	0.35	0.32
$Li_{1.3}Al_{0.2}\ Sc_{0.1}Ti_{1.7}(PO_4)_3$	2.69×10^{-4}	0.29	0.26
$Li_{1.3}Al_{0.1}\ Sc_{0.2}Ti_{1.7}(PO_4)_3$	4.26×10^{-4}	0.28	0.24
$Li_{1.3}Sc_{0.3}Ti_{1.7}(PO_4)_3$	7.28×10^{-4}	0.26	0.22

(0.36, 0.36, 0.25). The alternation of these two types of sites along the conduction channels forms a three-dimensional network over which rapid ion transport occurs via an interstitial mechanism. An analogous transport mechanism is observed in the case of the doped compounds, except that the sites that were "interstitial" sites I, the undoped compound are now partly occupied in the doped Li-richer compounds.

As the concentration of Sc^{3+} increases, unit cell volume and ionic conductivity increased. This experimental finding harmonizes to the variation of Li site energies along the respective Li ion migration pathways derived from bond valence models for the compounds with different co-dopants (see Fig. 7). The lattice expansion associated to a replacement of the small dopant ion Al^{3+}, by the isovalent larger dopant Sc^{3+} reduces both the activation energy for reaching the interstitial site and the site energy of this

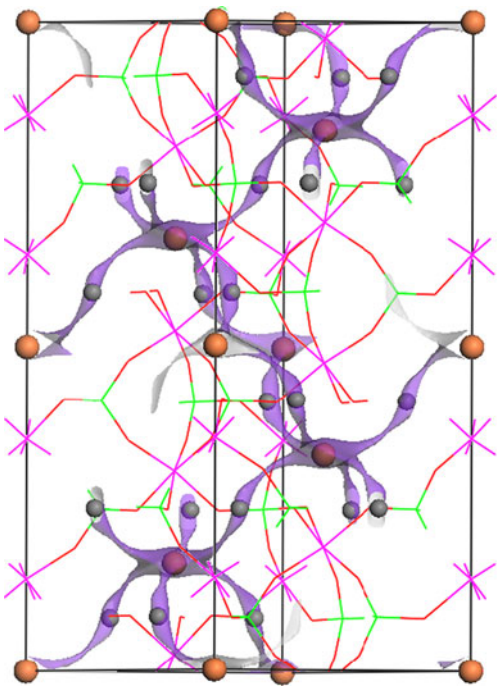

Fig. 6 Network of Li ion conduction pathways in undoped $Li_1Ti_2(PO_4)_3$ (*light spheres* regular Li site, *dark spheres* interstitial sites; isosurface indicates the continuous Li transport pathway accessible with an activation energy of 0.45 eV)

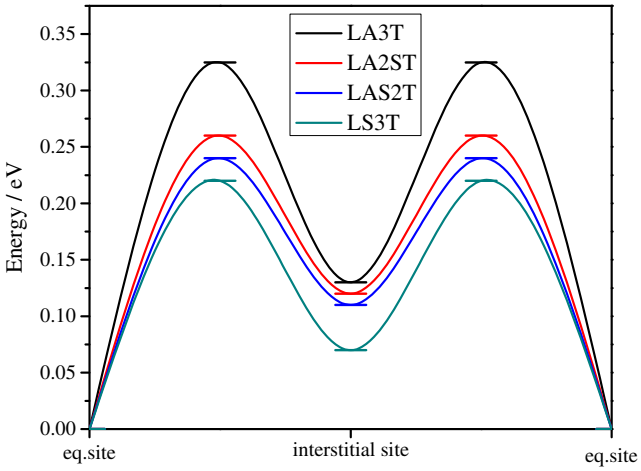

Fig. 7 Energy landscape for the motion of a Li ion along the BV-modelled Li pathways in the investigated Al, Sc co-doped NASICON phases $Li_{1.3}Al_xSc_{0.3-x}Ti_{1.7}(PO_4)_3$

interstitial. The activation energies calculated from the energy variation along these paths are semi-quantitatively in line with the experimental values (cf. Table 2). The high cation mobility and thermal stability of NASICON double phosphates allow us to regard them as potential materials for use in electrochemical devices. Obviously, the increase in unit cell volume due to the doping with the large Scandium ion facilitates Li^+ ion motion via increasing the free volume and—as already suggested by Bykov et al. [18]—widens oxygen windows, the critical bottlenecks for Li ion migration. Conductivity variations observed in this work are qualitatively in line with previous report, yet the conductivity values are lower than the values from an earlier report [19].

Summary

$Li_{1+x}Al_ySc_{x-y}Ti_{2-x}(PO_4)_3$ (x=0.3, y=0,0.1,0.2,0.3) NASICON compounds were prepared by mechanical milling followed by annealing of the samples. Among the investigated samples $Li_{1.3}Sc_{0.3}Ti_{1.7}(PO_4)_3$ with NASICON type structure showed highest ionic conductivity (~10^{-4} S/cm) and lowest activation energy 0.26 eV and has high thermal coefficient of expansion. BV analysis showed that in all these structures the Li ions fully occupy the regular I1 sites on the inversion centre coordinated by six oxygen atoms and partially occupy the I2 site that is a vacant interstitial site in the undoped $Li_1Ti_2(PO_4)_3$. The Li transport pathways connect two I1 sites via the I2 site. The alternation of these two types of sites along the conduction channels forms a three-dimensional network over which rapid ion transport occurs. While doping by the slightly smaller Al^{3+} essentially affects the concentration of interstitials, doping with Sc^{3+} expands the structure and thereby lowers the site energy of the I2 sites and the energy barriers along the path between

"interstitial" and regular Li sites. For the co-doped samples, the conductivity enhancement varies non-linearly with the volume expansion: a significant enhancement in conductivity is only achieved when the unit cell volume is increased to values beyond the volume of the undoped $Li_1Ti_2(PO_4)_3$.

Acknowledgement Financial support to authors in the frame of the Singapore Ministry of Education Grant MOE2009-T2-1-065 is gratefully acknowledged.

References

1. Fergus JW (2010) J Power Sources 195(15):4454–4569
2. Knauth P (2009) Solid State Ionics 180:911–916
3. Hong HYP (1978) Mat Res Bul 13:117
4. Fu J (1997) Solid State Ionics 104:191–194
5. Chowdari BVR, Subba Rao GV, Lee GYH (2000) Solid State Ionics 136-137:1067–1075
6. Adams S, Hariharan K, Maier J (1996) Solid State Ionics 86–88:503–509
7. Aono H, Sugimoto E, Sadaoka Y, Imanaka N, Adachi G (1990) J Electrochem Soc 137:1023–1027
8. Larson AC, von Dreele RB, General Structure Analysis System (GSAS); Report LAUR 86-748; Los Alamos National Laboratory: Los Alamos, NM, 2000
9. Alami M, Brouchu R, Soubeyroux JL, Gravereau P, le Flem G, Hagenmuller P (1991) J Solid State Chem 90:185–193
10. Adams S (2000) J Power Sources 159:200–204
11. Adams S (2001) Acta Crystallogr B, Struct Sci 57:278–287
12. Adams S, Swenson J (2004) Solid State Ionics 175:665–669
13. Adams S (2006) Solid State Ionics 177:1625–1630
14. Adams S, Rao RP (2009) Phys Chem Chem Phys 11:3210–3216
15. Rao RP, Tho TD, Adams S (2010) Solid State Ionics 181:1–6
16. Adams S, Rao RP (2011) Phys Stat Sol A 208(8):1746–1753
17. Rao RP, Adams S (2011) Phys Stat Sol A 208(8):1804–1807
18. Bykov AB, Chirkin AP, Demyanets LN, Doronin SN, Genkina EA, Ivanov-Shits AK, Kondratyuk IP, Maksimov BA, Melnikov OK, Muradyan LN, Simonov VI, Timofeeva VA (1990) Solid State Ionics 38:31–52
19. Kazakevičius E, Šalkus T, Selskis A, Selskienė A, Dindune A, Kanepe Z, Ronis J, Miškinis J, Kazlauskienė V, Venckutė V, Kežionis A, Orliukas AF (2011) Solid State Ionics 188:73–77